

ACE-ASIA

Regional Climatic and Atmospheric Chemical Effects of Asian Dust and Pollution

BY JOHN H. SEINFELD, GREGORY R. CARMICHAEL, RICHARD ARIMOTO, WILLIAM C. CONANT, FREDERICK J. BRECHTEL, TIMOTHY S. BATES, THOMAS A. CAHILL, ANTONY D. CLARKE, SARAH J. DOHERTY, PIOTR J. FLATAU, BARRY J. HUEBERT, JIYOUNG KIM, KRZYSZTOF M. MARKOWICZ, PATRICIA K. QUINN, LYNN M. RUSSELL, PHILIP B. RUSSELL, ATSUSHI SHIMIZU, YOHEI SHINOZUKA, CHUL H. SONG, YOUHUA TANG, ITSUSHI UNO, ANDREW M. VOGELMANN, RODNEY J. WEBER, JUNG-HUN WOO, AND XIAO Y. ZHANG

A large international field experiment and use of transport modeling has yielded physical, chemical, and radiative properties of the abundant aerosols originating from Asia.

No other region on Earth is as large and diverse a source of aerosols (and trace gases) as the Asian continent. In spring, when storm and frontal activity in Asia is most prevalent, industrial pollution, biomass burning, and mineral dust outflows produce an extraordinarily complex regional aerosol mix, composed of inorganic compounds (such as salts of

sulfates and nitrates), organic carbon (OC), black carbon (BC or soot), mineral dust, and water. Yet there are few data on the chemical, physical, and optical properties of Asian dust and pollution aerosols, especially as a function of altitude above the surface. Several important questions relevant to the chemical and climatic effects of Asian aerosol outflow remain to be

AFFILIATIONS: SEINFELD AND CONANT—Departments of Chemical Engineering and Environmental Science and Engineering, California Institute of Technology, Pasadena, California; CARMICHAEL, SONG, TANG, AND WOO—College of Engineering, University of Iowa, Iowa City, Iowa; ARIMOTO—CEMRC, New Mexico State University, Las Cruces, New Mexico; BRECHTEL—Brechtel Manufacturing, Inc., Hayward, California; BATES AND QUINN—NOAA Pacific Marine and Environmental Laboratory, Seattle, Washington; CAHILL—Department of Chemical Engineering, University of California, Davis, Davis, California; CLARKE, HUEBERT, AND SHINOZUKA—Department of Oceanography, University of Hawaii at Manoa, Honolulu, Hawaii; DOHERTY—Joint Institute for the Study of the Atmosphere and Oceans, University of Washington, Seattle, Washington; FLATAU—Naval Research Laboratory, Monterey, California; KIM—Meteorology Research Institute/KMA, Seoul, Korea; MARKOWICZ—Institute of

Geophysics, Warsaw University, Warsaw, Poland; L. M. RUSSELL AND VOGELMANN—Scripps Institution of Oceanography, University of California, San Diego, La Jolla, California; P. B. RUSSELL—NASA Ames Research Center, Moffett Field, California; SHIMIZU—National Institute for Environmental Studies, Tsukuba, Japan; UNO—Research Institute for Applied Mechanics, Kyushu University, Fukuoka, Japan; WEBER—School of Earth and Atmospheric Sciences, Georgia Institute of Technology, Atlanta, Georgia; ZHANG—Chinese Academy of Science, Beijing, China

CORRESPONDING AUTHOR: Dr. John H. Seinfeld, Mail Code 210-41, California Institute of Technology, Pasadena, CA 91125

E-mail: seinfeld@caltech.edu

DOI: 10.1175/BAMS-85-3-367

In final form 19 September 2003

©2004 American Meteorological Society

answered. For example: to what extent are dust and pollution particles internally mixed, and what impact does this have on their optical and hygroscopic properties? To what extent does dust serve as a surface for uptake of gases like SO₂ and HNO₃? Can chemical transport models simulate the optical properties and layering of different aerosol types sufficiently well to compute their chemical and radiative impacts?

From 5 to 15 April 2001, a massive dust storm occurred over the Asian mainland (Fig. 1) (Holden 2001). Dust storms in east Asia occur most frequently in the spring as a result of the combined effects of low rainfall, increased occurrence of high winds associated with cold fronts, and freshly tilled soil for spring planting. The dust outbreak of 5–15 April 2001 was among the largest on record, interrupting transportation schedules and disrupting daily activities. The position of the polar jet over midlatitudes, the associated strong surface winds, and the accompanying development of a midlatitude cyclone spawned the dust storm. The maximum surface winds during this time period occurred near 45°N, one of the major source regions for Asian dust.

At the time of this dust outbreak, the Asian Pacific Regional Aerosol Characterization Experiment (ACE-Asia) field studies were being conducted (information available online at <http://saga.pmel.noaa.gov/aceasia/>) (Huebert et al. 2003). While previous field experiments were conducted in the western Pacific to study the chemistry and aerosols coming off the Asian continent (Arimoto et al. 1996; Carmichael et al. 1996; Hayami and Carmichael 1998; Kim et al. 1998a,b), this international experiment, involving multiple aircraft, ships, satellites, and surface sites, obtained the most comprehensive measurements ever of hemispheric aerosol emis-

sion and transport. The data acquired during ACE-Asia allow a first-time assessment of the regional climatic and atmospheric chemical effects of a continental-scale mixture of dust and pollution. This article reviews what information is required to assess aerosol impacts over a continental or hemispheric scale, describes how ACE-Asia addressed the issues, and summarizes what the multidisciplinary studies showed.

PHYSICAL, CHEMICAL, AND OPTICAL PROPERTIES OF ASIAN AEROSOL.

Figure 2 shows estimated dust emissions (black areas) from eastern Asia over the period from 1 to 20 April 2001. Mineral particles are emitted into the atmosphere as a result of high surface winds and can be transported aloft through boundary layer convection and vertical motions associated with frontal boundaries. Natural

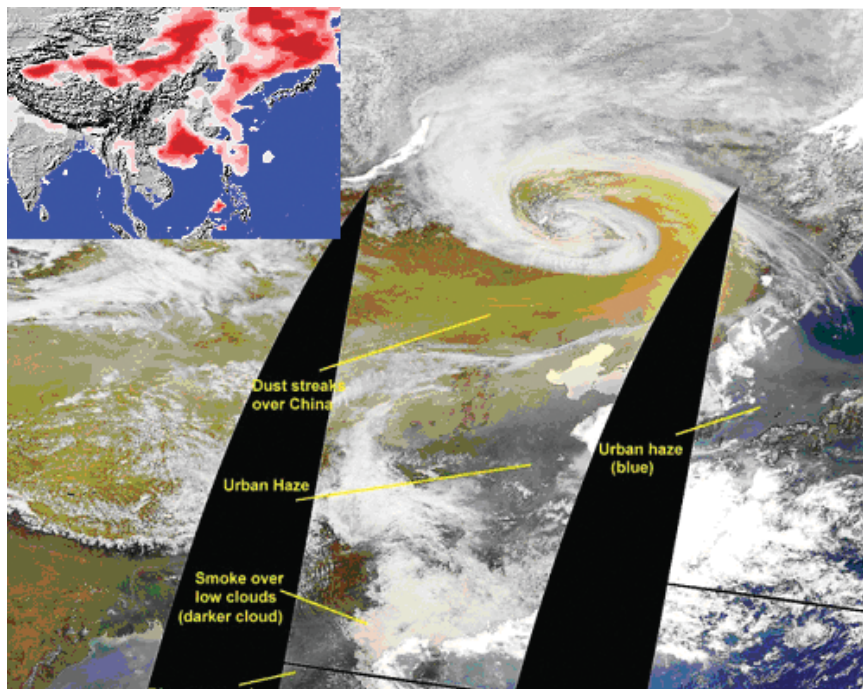


FIG. 1. The Sea-viewing Wide Field-of-View Sensor (SeaWiFS) image for 7 Apr 2001 illustrates the complexity of the aerosol distributions during large dust storms. Dust (shown in yellowish brown) is transported, along with the intense low pressure system, horizontally and vertically into the center of the low. Ahead of the front, urban pollution (brownish gray area south of the dust) is transported across Korea and Japan. During this period, widespread fires were burning in Southeast Asia, and carbonaceous aerosols associated with these fires were transported away from the continent and toward Japan in the warm sector ahead of this large cold front. Over the Pacific, these aerosols are higher than the clouds. The composite TOMS aerosol index (AI) for 7–9 Apr 2001 (upper left corner) is indicative of absorbing aerosol (either dust or black carbon). The high values of AI (indicated by dark red) over east Asia are due to dust, while those in Southeast Asia are due to biomass burning. The TOMS image shows clearly the two waves of dust associated with the storm.

dust emission areas are defined as desert and semi-desert areas in the United States Geological Survey (USGS) vegetation database [based on Advanced Very High Resolution Radiometer (AVHRR) data obtained in 1992/93]. By using this method, large parts of the Gobi and Taklimakan Deserts are indexed as source regions. The Loess Plateau and the Nei Monggol's small desert were further assigned as dust source areas based on Total Ozone Mapping Spectrophotometer (TOMS) aerosol index (AI) climatologies. Snow cover data are used to mask predicted emission areas (e.g., many parts of the Himalayan mountain range), providing a seasonal element to dust emissions. Complete details of the algorithm used in estimating the dust emissions can be found in Uno et al. (2003).

Approximately 50 teragrams (Tg) of dust is estimated to have been emitted during this period from the arid and semiarid regions of western China, northern China and Mongolia, the loess regions west of Beijing, China, and the drought-stricken regions in Liaoning Province (northeast of Beijing) (Uno et al. 2003). The BC emissions from biomass burning (red areas in Fig. 2) during this same period are estimated

as ~ 0.05 Tg, with an additional 0.1 Tg from fossil and biofuel combustion. Emission rates of BC from biomass burning were based on regional estimates of biomass burned and AVHRR fire counts. Fossil and biofuel emission estimates are based on Streets et al. (2001). Sulfur emissions from combustion are estimated as 0.95 Tg (S).

Aerosols collected in the dust source region near Zhenbeitai, China ($38^{\circ}37'N$, $109^{\circ}46'E$; see Fig. 2), established the elemental composition of the dust. These samples were collected during April 2001 over nominal 24-h intervals using an Interagency Monitoring of Protected Visual Environments (IMPROVE)-type sampler, operating at a flow rate of ~ 11.5 l min^{-1} . Acid digests (HF, HCl, and HNO_3) of the GN-4 Metrical filters (Pall Gelman Sciences, Inc.) were analyzed by inductively coupled plasma mass spectroscopy. The ratios of 25 elements (Al, Ba, Ca, Ce, Co, Dy, Er, Eu, Fe, Gd, K, La, Li, Mg, Mn, Na, Nd, Pr, Sc, Si, Sm, Sr, Th, Ti, and U) to Al in the aerosol samples were within 30% of those certified or measured in a loess reference material (Nishikawa et al. 2000), demonstrating a chemical connection between the dust and eolian

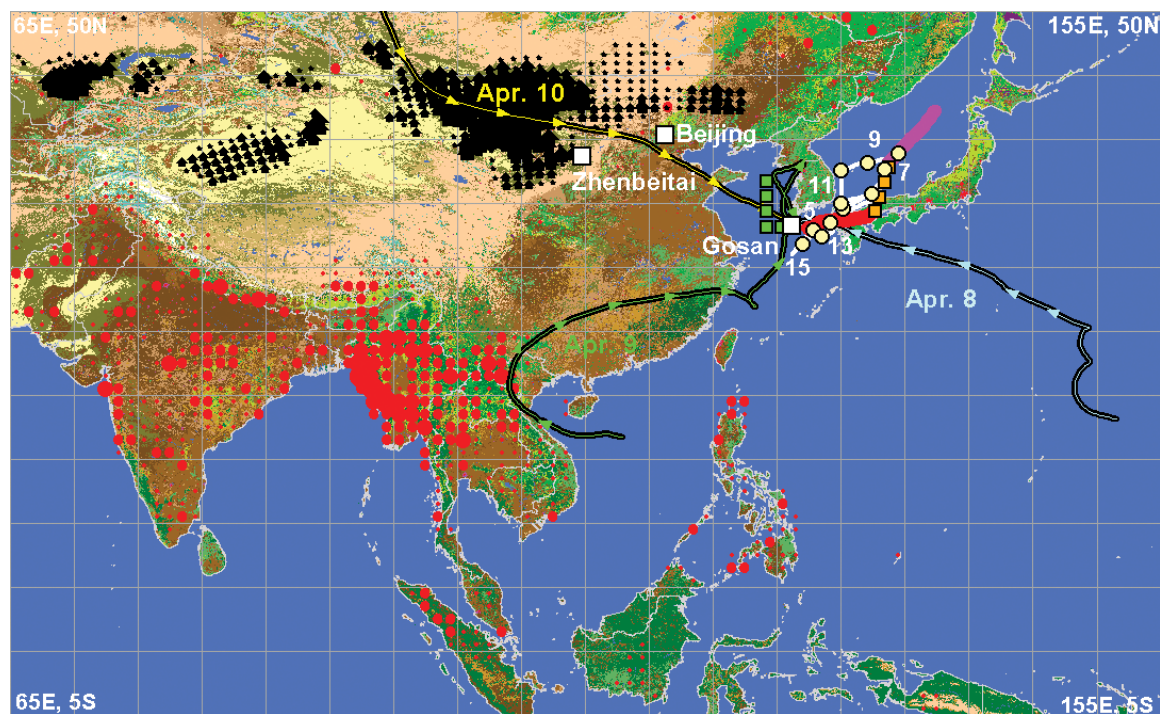


FIG. 2. Dust emissions fluxes (black) and AVHRR fire counts (red) over the period 1–20 Apr 2001. Surface measurement sites discussed in the text are shown, along with the location of the R/V *Ronald H. Brown*, and the flight tracks of the C-130 and Twin Otter aircraft on 8 and 12 Apr. Numbers next to the tracks indicate Apr dates. Near-surface three-dimensional trajectories were calculated by the RAMS meteorological model, as described in Uno et al. (2003). At the time that the R/V *Ronald H. Brown* observed the dust storm on 11 Apr it was positioned near the tip of South Korea, where trajectories were very similar to those at Gosan.

sedimentary material. In contrast, a second group of elements (Ag, Bi, Cd, Cr, Cu, Hg, Mo, Ni, Pb, Sb, Tl, V, and Zn) was uncorrelated with Al, and these elements displayed ratios to Al ranging from 6 to 100 times those expected from the Asian mineral dust standard, most likely reflecting pollutant emissions (Nriagu and Pacyna 1988). The detection of Tl is especially noteworthy because Tl is emitted by coal-fired power plants, smelting operations, and cement plants, all of which are important sources of pollutants in Asia. These elemental data indicate that even in the dust source region itself, significant quantities of pollutants can become mixed with the mineral dust.

Lidar images of the normalized aerosol backscatter, extinction coefficient, and depolarization ratio at Beijing show the advance of the storm over 6–15 April (three left panels of Fig. 3). Automated Mie scattering lidar (Sugimoto et al. 2003) was used to determine vertical profiles of backscattering intensities and depolarization ratios. Extinction coefficients for 532 nm were derived using Fernald’s method (Fernald 1984). Lidar measurements of atmospheric depolarization can be used to distinguish between spherical and nonspherical particles. The depolarization ratio of a linearly polarized laser beam backscattered from spherical particles is zero, so the

magnitude of the ratio is indicative of the amount of nonspherical (in this case, dust) particles. The early April dust storm consisted of two distinct events. Dust (as indicated by the region of enhanced depolarization) arrived over Beijing in a layer between 2 and 4 km on 6 April, where it overrode a sulfate-rich pollution layer (as evidenced by high backscatter and extinction in this near-surface layer). The dust layer descended to the surface during 7–8 April when optical extinctions reached values up to 0.3 km^{-1} . After the dust-overriding pollution layers passed on 8 April, a new pollution layer, rich in sulfate and carbonaceous aerosol, was transported from southwestern China to Beijing (as seen by the high extinction and backscatter early on 9 April). The second dust wave reached Beijing on 9 April. Dust in the leading edge of this front extended up to 6 km; behind the front the dust was confined largely to heights below 2–3 km, where it was mixed with polluted air, as shown by the model results where the enhanced observed extinction in the boundary layer on 10 April is attributed to high levels of BC, sulfate, and dust.

During ACE-Asia, several global and regional chemical transport models were used in the field to help in mission planning. One such model was the Chemical Weather Forecast System (CFORS; Uno

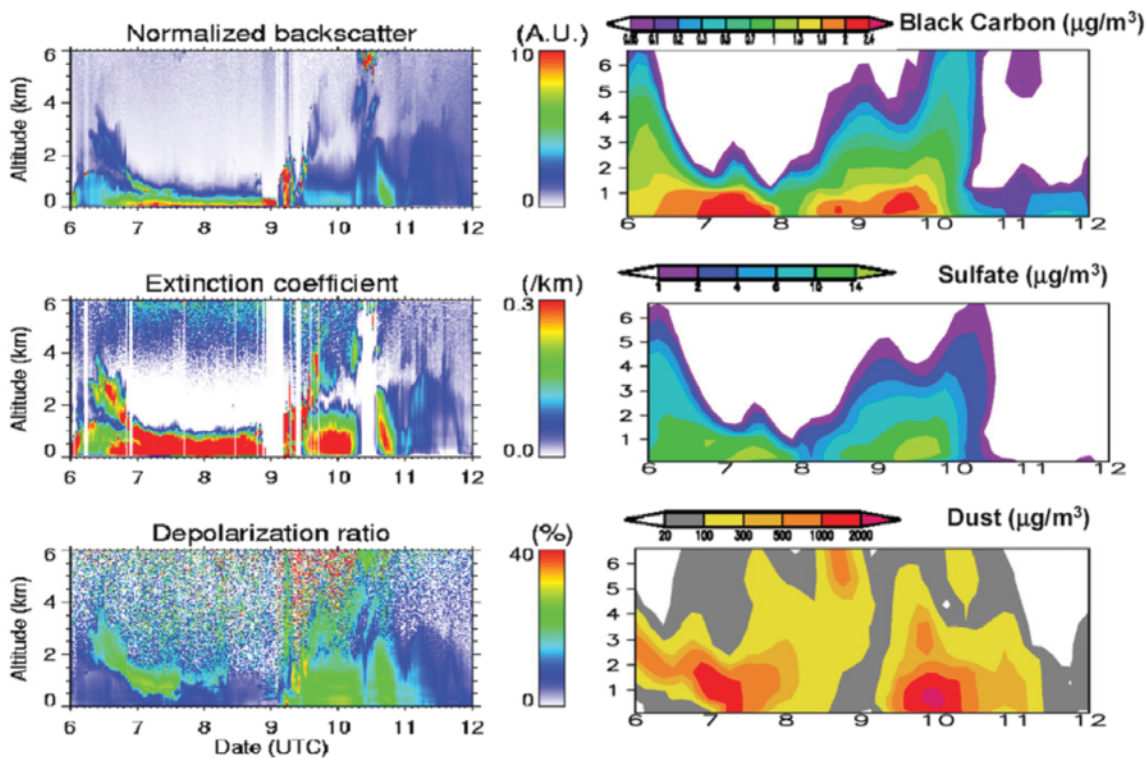


FIG. 3. (left) Lidar images over Beijing. (right) Time–height profiles of calculated mass distributions of (bottom) dust, (middle) sulfate, and (top) black carbon for Beijing using the CFORS model. Abcissa shows data (UTC) indicating day in Apr 2001.

et al. 2003). CFORS is a multitracer, online system built within the Regional Atmospheric Modeling System (RAMS) mesoscale meteorological model (Pielke et al. 1992). In CFORS multiple tracers are run online in RAMS, so that all the online meteorological information, such as 3D winds, boundary layer turbulence, surface fluxes, and precipitation amount, are available at every time step to produce high-time-resolution 3D tracer fields. CFORS treats size-resolved mineral dust using 12 particle bins (ranging from 0.1 to 20 μm in radius) and a wide variety of tracers: 1) important anthropogenic species (SO_2/SO_4 , CO, black carbon, organic carbon, fast and slow reacting hydrocarbons, and NO_x), 2) species of natural origin (yellow sand, sea salt, radon, volcanic SO_2), and 3) markers for biomass burning (CO, black carbon, and organic carbon). The three right-hand panels of Fig. 3 show the vertical distributions of black carbon, sulfate, and dust over Beijing as predicted by the CFORS chemical transport model. The two events composing this dust storm stand out in the 3-day composite TOMS aerosol index insert in Fig. 1. Over the course of the next 3–4 days, the wave of dust moved eastward away from the coast of China and was sampled aloft by aircraft and at numerous surface sites.

During the 9–13 April dust storm, several research flights were conducted by the National Science Foundation C-130 and U.S. Navy Twin Otter to characterize the vertical profiles of aerosol extinction, mass, and size. On 8 April, over the Sea of Japan, during the same dust storm observed at Zhenbetai and Beijing, the C-130 repeatedly flew in and out of an elevated river of dust rich in calcium, situated above a sulfate-rich pollution plume located near the surface downwind of the Korean peninsula. These two aerosol fields were separated by an intermediate pollution layer near the temperature inversion at ~ 2.5 km. The observed complex structure was not uncommon and is best visualized in 3D plots of key parameters during the flight (Fig. 4); the complexity also demonstrates the challenges faced by three-dimensional atmospheric chemical transport models.

Total extinction of incoming radiation by aerosols is the sum of scattering and absorption. The aerosol-scattering data in Fig. 4a obtained over the Sea of Japan reveal highest values near 4-km altitude to the north of the region, while aerosol absorption (Fig. 4b) is at a maximum near the surface to the south. The aerosol single scattering albedo (SSA; the ratio of incident radiation scattered to total extinction) is the commonly used measure of the relative contribution of absorbing aerosol to extinction and is a key variable in assessing the climatic effect of the aerosol. Its

value depends both on the concentration and size distribution of absorbing substances and how these are mixed with nonabsorbing aerosol material (Jacobson 2000). The strongest particulate absorber is BC; iron compounds present in dust also absorb shortwave radiation. The effective refractive index for average Asian dust was constrained by the asymptotic value of coarse absorption per unit volume as coarse volumes approached maximum values. This assessment included size-resolved corrections for soot associated with the coarse mode and for impactor transmission efficiency for a nominal size cut at 0.75 μm . The resulting dust refractive index was determined to be $1.53 - 0.0007i$ (± 0.0002) (Y. Shinozuka 2003, personal communication). The range of dust distributions measured during ACE-Asia yield calculated SSA values larger than 0.99 for submicrometer dust and about 0.97 ± 0.02 for coarse dust at 550-nm wavelength. The latter is also consistent with bulk SSA values inferred from differences between measured total and submicrometer scattering and absorption.

The SSA (Fig. 4) approaches 0.97 in the upper levels of the north, where total extinction is completely dominated by scattering associated with dust, and about 0.85 near the surface to the south, where southwesterly transport of carbonaceous aerosol from regions impacted by biomass burning leads to a significant absorbing component. This high SSA for the dust-dominated aerosol aloft is consistent with recent similar values for Asian dust plumes crossing the Pacific and has been observed being entrained into the marine boundary layer (Clarke et al. 2001). These and similar cases observed aloft on the C-130 indicate that lower SSA values often found in the presence of Asian dust measured near the surface are generally a result of absorption by BC present in the accumulation (0.1–1.0- μm diameter) mode.

The ratio of the particle wet diameter at a given relative humidity (RH) to its dry diameter [denoted as $f(\text{RH})$] is a measure of the amount of water that is taken up by the aerosol as RH increases. This property is important because particle swelling associated with increasing RH can strongly affect the scattering of solar radiation as the aerosol moves through different ambient conditions. This measured hygroscopic growth factor $f(\text{RH})$ from RH = 40% to RH = 80% (Fig. 4d) ranges from near unity aloft, where it indicates negligible growth due to water uptake by dust, to a maximum of 2.5 near the surface, indicative of strongly hygroscopic aerosol (e.g., NaCl). The elevated layer to the north exhibited high aerosol Ca^{2+} (Fig. 4e), associated with large, coarse aerosol volumes (or mass) (Fig. 4g), both indicative of dust. In con-

trast, the highest aerosol sulfate is evident near the surface to the south where submicrometer aerosol

volume (or mass) is at a maximum (Fig. 4h). The elemental composition measured at 4 km by the C-130

on 8 April shows submicrometer aerosol composition, similar to that collected near Zhenbeitai, with nine elements (Al, Ca, Fe, K, Mg, Mn, Na, Sr, and Ti) within 30% of the loess-certified reference material. A contrasting group of six elements (Cr, Cu, Ni, Pb, V, and Zn) indicated the presence of pollutants with ratios relative to Al that were enhanced over this dust composition by factors of 3 or more.

The data in Fig. 4 reveal the close coupling between aerosol physical chemistry and associated optical effects. The upper-level dust layer, with up to $1200 \mu\text{g m}^{-3}$ of dust (Fig. 4g; from $600 \mu\text{m}^3 \text{m}^{-3}$, assuming a density of 2g cm^{-3}), has a total dry scattering intensity of near 200Mm^{-1} (Fig. 4a). In contrast, the lower-altitude pollution plume has a pronounced accumulation mode volume (Fig. 4g) with a mass of about $30 \mu\text{g m}^{-3}$, including about $10 \mu\text{g m}^{-3}$ of soluble sulfate (Fig. 4f) and other associated components, and exhibits dry scattering near 100Mm^{-1} (Fig. 4a). However, when the differences in hygroscopic growth at the same RH are taken into account, the lower-level soluble aerosol produces an ambient scattering close to 200Mm^{-1} , similar to that of the upper-level dust layer.

Even within the elevated dust layer, sampling at 4-km altitude revealed the significant presence of submicrometer carbonaceous aerosol. The organic carbon was dominated by saturated alkyl groups with an organic mass-to-organic carbon ratio of 1.3, resulting from absorption by oxygenated groups. Organic mass-to-organic carbon ratios are based on composite analysis of organic functional groups in submicrometer particles by Fourier transform infrared spectroscopy (Maria et al. 2002). Elemental composition was determined by x-ray fluores-

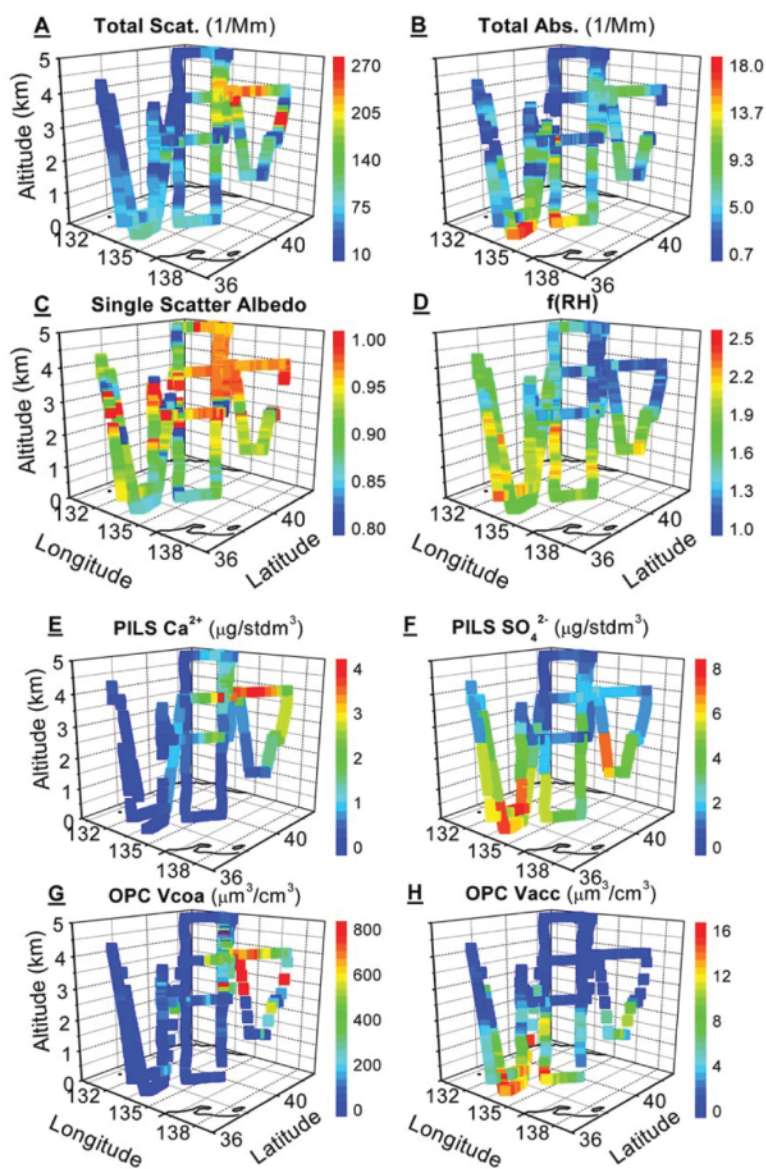


FIG. 4. Measurements aboard the NCAR C-130 on 8 Apr in the dust cloud over the Sea of Japan. This eight-panel plot is arranged into four panels of measured aerosol optical characteristics at 550 nm [(a) total aerosol light scattering, (b) total aerosol light absorption, (c) aerosol single scattering albedo, (d) $f(\text{RH})$, see text] and (e)–(h) four panels of the physiochemical properties that give rise to these characteristics. Observed aerosol (e) Ca^{2+} and (f) SO_4^{2-} as a function of altitude along the flight track are based on rapid and continuous measurements with a new instrument (PILS) that captures particles ($\leq 1.5\text{-}\mu\text{m}$ diameter) directly into a small flow of purified water (Weber et al. 2001). Although the predominance of calcium occurred in larger particles (total calcium reached 19,000 pptv versus only 1600 pptv in particles $\leq 1.5 \mu\text{m}$), the PILS data are still a reliable indication of dust because the tail of the dust distribution goes below $1.5 \mu\text{m}$. (g) Coarse and (h) fine aerosol components, separated at aerodynamic particle diameter of $1 \mu\text{m}$, are shown here as “dry” volumes as measured.

cence of submicrometer particles on stretched Teflon filters. Trajectory analysis suggests this aerosol originated from biomass burning in Southeast Asia. The lower-altitude carbonaceous aerosol was less aged and more closely correlated with local combustion-derived emissions of sulfate.

In the above case, the river of dust near 4 km was largely isolated from the pollution layer. When intermingling occurs, complex interactions are possible. For example, high SO_2 and favorable conditions have resulted in estimated sulfuric acid production in the range from 0.2 to $1 \times 10^6 \text{ cm}^{-3} \text{ s}^{-1}$ over the Yellow Sea (Weber et al. 2003). Under certain conditions, the H_2SO_4 can lead to production of new particles. The H_2SO_4 also rapidly deposits on particles, and such fluxes are consistent with observed measurements of aerosol growth. Sulfate and nitrate coatings on dust sampled in Beijing and Qingdao have been found to change the properties of dust, such as its hygroscopicity. Evidence of nitrate coatings on dust has also been observed in this region (Weber et al. 2001; Orsini et al. 2003). In the absence of dust, gas-to-particle conversion of sulfates and nitrates will occur on accumulation-mode particles; thus, when dust is present, gas-to-particle conversion affects both sub- and supermicrometer aerosol modes by redirecting much of the deposition that would normally occur on the accumulation mode to the larger dust particles.

Shipboard measurements on the R/V *Ronald H. Brown* in the Sea of Japan (see *Ronald H. Brown* track in Fig. 2) complemented those of the C-130 during this episode (Fig. 5). Aerosol optical thickness (AOT, the integral of the aerosol extinction coefficient from the surface to the top of the atmosphere) exceeded 1.4 on 10 April (top left panel). On this day, emissions from the Miyakejima volcano (located 200 km south of Tokyo) were transported into the Sea of Japan, and elevated sulfate in this plume caused the enhanced extinction below 1000 m shown in the extinction panel in Fig. 5. Above 4 km, dust emitted from the Taklimakan region passed over the ship and contributed to the elevated aerosol optical thickness. (The SO_2 emissions from the Miyakejima volcano are estimated to be $1.5 \times 10^{10} \text{ g S day}^{-1}$ during this period, an amount that was 50% of *total* anthropogenic sulfur emissions in East Asia.) At the sea surface, the SSA was 0.98, and the aerosol was dominated by sulfates (up to $30 \mu\text{g m}^{-3}$) and organics. The arrival of the second dust peak on 11 April at the ship was revealed by increases in total aerosol Al and Ca, peaking at ~ 13 and $7 \mu\text{g m}^{-3}$, respectively, on 12 April (top right panel). In this low-level outflow, the submicrometer

portion of the dust, as determined by the measured ratio of sub- to supermicrometer Al and Ca, was significant (15%–30%). The two lower panels of Fig. 5 show aerosol extinction and total dust at the location of the ship, as predicted by the CFORS model.

Surface observations of particle number size distributions at Gosan, Korea (Fig. 6), also reveal the eastward progression of the dust event that arrived in Beijing early on 10 April. For descriptions of the instrumentation used see Brechtel and Buzorius (2001) and Chun et al. (2001). Just before 0000 UTC 11 April, a striking increase in supermicrometer aerosol number concentration marks the arrival of the dust storm at Gosan, which lasted 3 days. The same two extinction maxima observed at Beijing on 8 and 10 April can be seen in the two-course mode maxima in the size distribution at Gosan on 10 and 12 April. The transported aerosol reflected a mixture of pollution and dust with increases in super- and submicrometer mode area concentrations of 164% and 45%, respectively, compared to study averages and significant changes to ambient light extinction.

The ACE-Asia project design established a network of surface sites that, with additional collaborators, covered approximately 40% of the earth's circumference. Size-resolved particle composition was measured at 15 sites, with 3-h time resolution. A sequence of data at the Tango site, north of Kyoto, Japan, on a peninsula jutting into the Sea of Japan (see Fig. 2) from the 10-day period spanning the dust event (Fig. 7) complements the data presented above. Samples were analyzed for mass (soft beta ray), optical transmission versus wavelength (320–820 nm), and elements (Na and heavier) by synchrotron x-ray fluorescence. Air trajectories arriving at Tango are similar to those shown in Fig. 2 for Gosan, Korea. Early in the event the air masses at Tango swept over central Japan and then abruptly switched direction and speed to reflect rapid transport of dust from the Taklimakan Desert. During the mid-April dust event, observations at numerous surface sites along the path of the dust storm demonstrate that optically important aerosols and coated dust particles, as well as primary and secondary anthropogenic aerosol, cross the study region into the North Pacific and were detected as far away as Oregon (VanCuren and Cahill 2002).

Heterogeneous reactions involving SO_2 , NO_2 , and O_3 on metal oxides and Chinese loess soils, in addition to direct deposition of H_2SO_4 and HNO_3 , have been observed in the laboratory (Michel et al. 2002). As a result of the reaction of HNO_3 with Ca^{2+} , the size of the aerosol nitrate was well correlated with that of soluble Ca during the postfrontal outflow of this dust

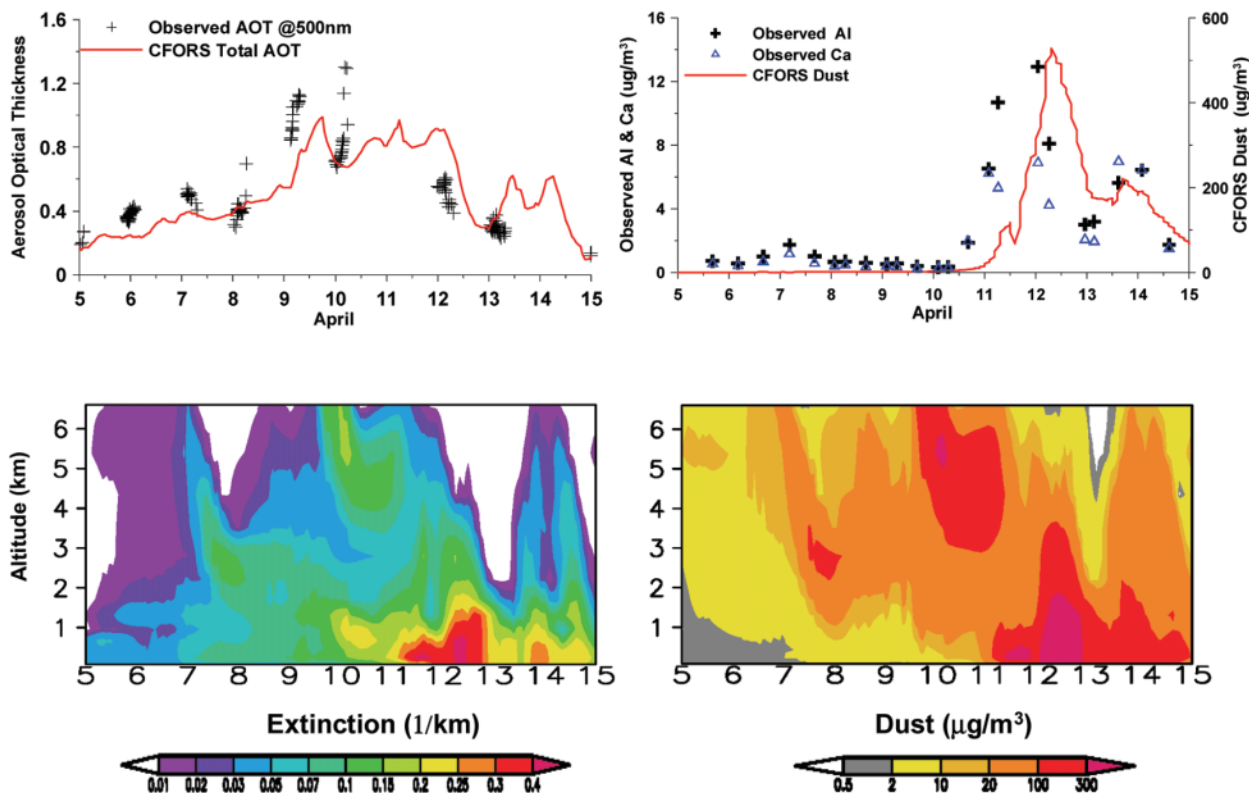


FIG. 5. (top left) Measurements of AOT on the R/V *Ronald H. Brown* over 5–15 Apr show values exceeding 1.0 during the height of the dust storm. (top right) Al and Ca, measured onboard, also peak at this time. In most cases model predictions follow these data closely. (bottom) Predicted vertical distributions of (left) aerosol extinction and (right) dust concentrations are shown corresponding to the *Ronald H. Brown* cruise track.

storm. Over the course of the project, just over 75% of the nitrate was on particles larger than $0.8 \mu\text{m}$ (B. Huebert 2002, unpublished manuscript). While some sulfate (up to 30%, but usually less than 5%) was also found in the larger particles, its size distribution typically peaked in the submicrometer range, where it was most strongly correlated with ammonium. This aerosol state apparently evolves from both the uptake of recent photochemically formed acidic gases and the progression of the urban aerosol to a more stable thermodynamic state when mixed with alkaline dust. Measurements show that fresh urban plumes, identified by high SO_2 concentrations, when blended with the dust in the postfrontal outflow, contained fine particles of ammonium sulfate and nitrate salts, and coarse alkaline dust (CaCO_3), with some $\text{Ca}(\text{NO}_3)_2$. However, outside these fresh plumes, the more aged dust and pollution plumes still contain fine ammonium sulfate salts, but lack fine nitrate, suggesting that $\text{Ca}(\text{NO}_3)_2$ was formed through the evaporation of the semivolatile ammonium nitrate. Thus, the different size distributions of sulfates and nitrates are attributable in part to the fact that SO_2 reactive uptake coef-

ficients on metal oxides are roughly 0.1–0.01 of those for HNO_3 , especially under dry conditions (Grassian 2001), and that over time the plumes evolve to the most stable chemical forms. The reaction of nitric acid with calcareous dust particles is important because it provides a pathway to the formation of calcium nitrate, which is hygroscopic. Water uptake by dust particles increases their interaction with solar radiation and renders them effective cloud condensation nuclei (CCN).

Large quantities of aerosols are transported out of the region by these dust events. We estimate, using a three-dimensional model (Uno et al. 2003) that approximately 14 Tg of dust, 0.4 Tg of sulfates, and 0.5 Tg of carbonaceous aerosol were transported eastward across 130°E during the 5–15 April period, representing 28% and 42% of the total dust and sulfate emissions, respectively, in the region. These percentages reflect the preferential removal of dust relative to sulfates, which is consistent with the larger size of the dust particles. In Beijing alone, we estimate that $\sim 67,000$ tons of dust were deposited over the 11-day period of the dust storm. The flux of dust deposited to the ocean surface is estimated as 2.4 Tg during 5–

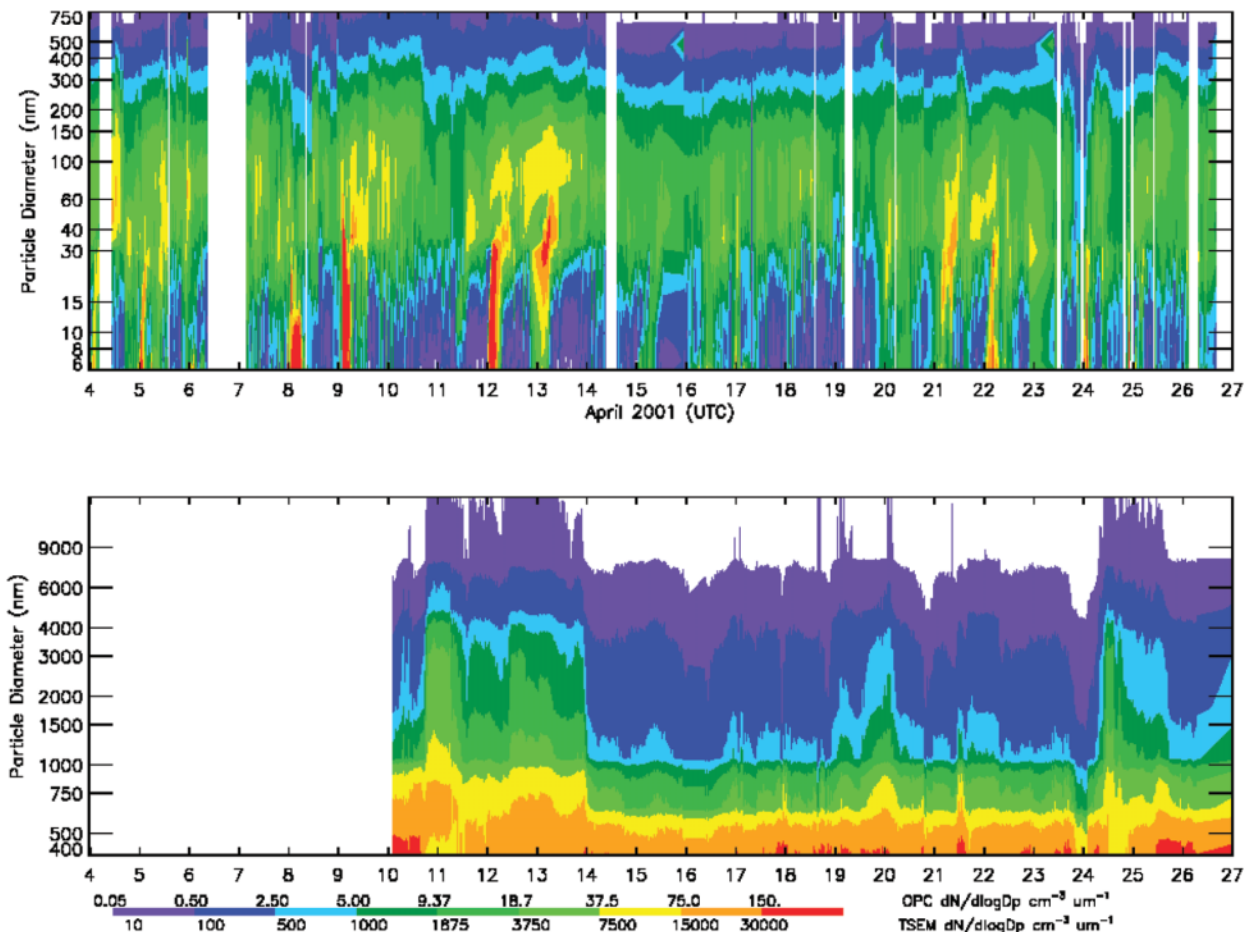


FIG. 6. (top) Electrical mobility and (bottom) optical particle (OPC) number size distributions measured at Gosan. Data are shown as timelines with particle size on the ordinate, time on the abscissa, and color contours representing the number concentration at a given size. Three distinct dust events on 10–13, 19, and 24–25 Apr are evident in the coarse mode OPC data, with simultaneous decreases in submicrometer number concentrations, especially for particles larger than 150 nm and smaller than 30 nm. The noted behavior in the submicrometer range may be attributable to precipitation scavenging of particles in air heavily influenced by cloud processing in the frontal boundary transporting the dust.

15 April and 8.7 Tg during all of March and April. Based on the measured dust composition of 4% Fe at Zhenbeitai, 0.1 Tg (Fe) (100,000 tons) was present in the dust during the dust storm and 0.35 Tg (Fe) for the spring of 2001.

RADIATIVE ENERGY BALANCE OVER THE WESTERN PACIFIC.

Unlike the long-lived greenhouse gases (GHGs), which tend to spread uniformly over the globe, tropospheric aerosols have a lifetime of about 1 week, resulting in a distribution that is spatially and temporally inhomogeneous. In further contrast to GHGs, perturbations to the earth's energy balance (radiative forcing) resulting from aerosols largely occur over and downwind of industrialized areas of the Northern Hemisphere, with significant impacts on regional energy budgets, evapo-

ration, and precipitation. Regional aerosol forcings are often one order of magnitude larger than those of the GHGs (Ramanathan et al. 2001).

For aerosols that exclusively scatter solar radiation, the increase in the reflected solar flux at the top of the atmosphere (TOA) is virtually identical to its reduction at the surface, and, as a result, both the surface and the atmosphere cool. For particles that both scatter and absorb solar radiation, such as black carbon and mineral dust, the amount of solar radiation reaching the earth's surface is likewise reduced, but the absorption of energy by these aerosols can heat the atmosphere as well. Absorption of radiation by aerosols in the lower atmosphere, at the expense of absorption at the surface, may affect the temperature profile, atmospheric stability, and relative humidity, all of which influence atmospheric dynamics and cloud formation.

Radiative transfer calculations, using a Monte Carlo radiative transfer model (MCRTM) based on the predicted CFORS aerosol distributions, measured SSA, and climatological cloud conditions indicate that during the period of the dust outbreak aerosols cool the surface by 14 W m^{-2} and heat the atmosphere by 11 W m^{-2} , resulting in a net climate forcing of -3 W m^{-2} over the region spanning 20° – 50°N , 100° – 150°E (Table 1). Podgorny et al. (2000) and

Vogelmann et al. (2001) provide details on the radiative transfer code. The solar spectrum is divided into 38 wavelength bands from 0.2 to $4.0 \mu\text{m}$. Aerosol optical properties used in MCRTM were determined from available observations of aerosol physical, optical, and chemical properties made during ACE-Asia combined with standard aerosol optical properties (Hess et al. 1998; Kaufman et al. 2001). The single-scatter albedo of pure dust at 500 nm is 0.98, derived from ACE-Asia in situ measurements. Calculations represent a mean from 5 to 15 April for the region 20° – 50°N , 100° – 150°E .

These calculations corroborate two major findings from other recent field campaigns conducted in the North Atlantic (Russell et al. 1999; Raes et al. 2000), Brazil (Eck et al. 1998), and the north Indian Ocean (Ramanathan et al. 2001; Satheesh and Ramanathan 2000). First, aerosol cooling can be comparable to or greater than human-induced greenhouse gas warming of 2 – 3 W m^{-2} over vast regions downwind of anthropogenic aerosol sources. Second, and more importantly, aerosols can exert a far greater influence on the surface and atmospheric energy budgets than on the TOA radiation budget because of their strong light-absorbing component (mainly black carbon).

When BC is present, the mixing state of the atmospheric aerosol can have a profound effect on its radiative properties. Black carbon, which comprises approximately 6% of the submicrometer aerosol mass, may remain entirely separate from other particles, or it may be mixed into them. This includes mixing in predominantly sulfate/OC aerosols and/or in mineral dust particles. To examine the sensitivity of radiative forcing to the state of aerosol mixing, we assume either that BC is separate or that 96% of the BC is internally mixed with sulfate/OC and 4% is internally mixed with dust (Table 1). The coating of dust is calculated based on electron microscope analyses of Asian dust (Gao and Anderson 2001) that find a prominent “coated” mode of dust particles

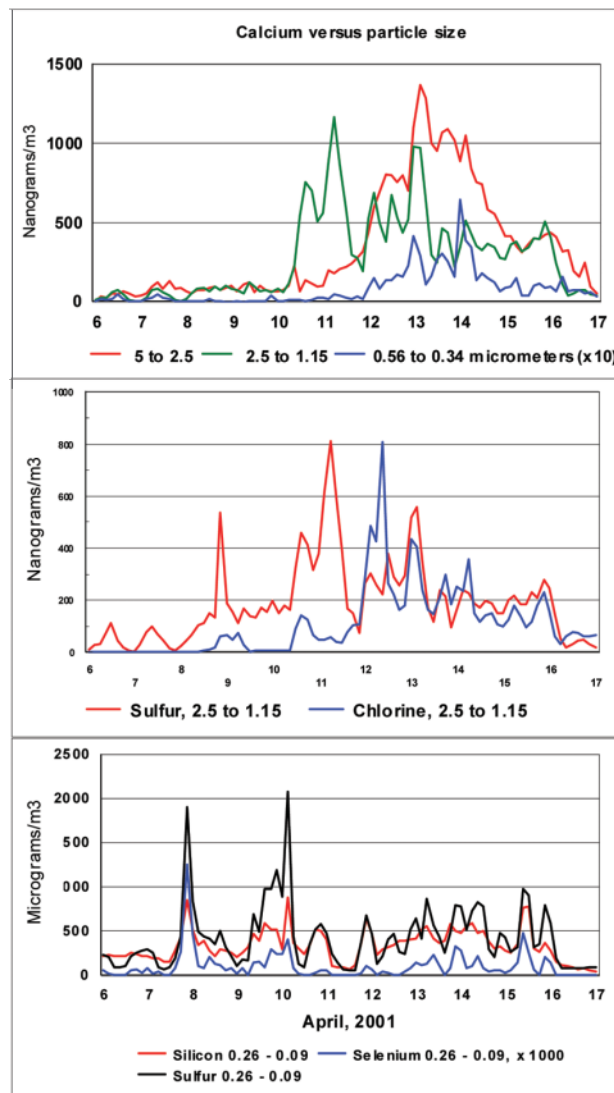


FIG. 7. Aerosol composition measured in several of the eight size ranges at the Tango site on the north coast of Japan. Air trajectory analyses show that five major source regions contributed to the observed data: 6–9 Apr slow trajectories over the Japanese inland sea; 10–11 Apr, same as the previous case plus the erupting volcano on Miyakejima, south of Tokyo; 12 Apr, a fast trajectory (6000 km in 4 days) from Siberia over the Taklimakan Desert in western China, and then over much of northern China; 13–14 Apr, somewhat slower trajectories from the Gobi Desert over Manchuria and Korea; and 15–16 Apr, slow trajectories from Beijing and Qingdao. (top) Calcium in three size modes, with the smallest size mode multiplied by 10. (middle) Calcium closely associated with sulfur in the same size mode, with relatively little silicon is a fingerprint for the Miyakejima volcano. The sharp increase in chlorine on 12 Apr resulted from sea salt NaCl transported in the high-wind regime to the site 6 km inland. Gobi dust arrived with anthropogenic elements and the highest accumulation mode sulfur seen in the entire 42-day experiment. (bottom) Highly correlated elements in the very fine mode (0.29 – $0.09 \mu\text{m}$) previously seen in studies of coal-fired power plants in the western United States.

having a S:Si ratio of 2:50. Thus, each dust particle is coated with a 2.7% (by mass) layer of sulfate, organic carbon, and black carbon. Given that Si is assumed to comprise 26% of the dust mass, sulfur is assumed to be ammonium bisulfate, and OC and BC in the coating are taken from an assumed mass proportion of sulfate:OC:BC equal to 32:18:3. Under cloud-free conditions, when the aerosol is internally mixed, the predicted impact is an increase of aerosol absorption by 3.5 W m^{-2} relative to the externally mixed case (see Table 1), resulting in a change in surface flux of -2.2 W m^{-2} and a net change in TOA forcing of 1.3 W m^{-2} .

Clouds moderate the TOA forcing by aerosol scattering, and can either magnify or reduce the heating by aerosol absorption, depending on surface reflectivity and the vertical profile of aerosols relative to clouds. Climatological satellite data were used to constrain the regional albedo and the vertical distribution of clouds in MCRTM. The clouds present are predicted to moderate the TOA forcing by a factor of ~ 3 compared to clear-sky calculations, whereas atmospheric absorption remains virtually unchanged. The predicted surface-to-TOA forcing ratio increases from 2.2 in the cloud-free case to 4.7 in the cloud-inclusive case.

Ship and satellite observations of clear-sky radiative forcing support the regional predictions described above. Radiative forcing can be expressed as the product of two measured quantities: aerosol optical thickness and aerosol forcing efficiency (change in radiative flux per unit optical depth at 500 nm). Shipboard (R/V *Ronald H. Brown*) observations of these quantities show that the aerosol radiative forcing efficiency at the ocean surface varied from -50 to below -80 W m^{-2} . The forcing is very sensitive to variations in aerosol composition—the days with the strongest forcing efficiencies were those with highest BC content (lowest SSA). Mean 500-nm AOT in the Sea of Japan (7–13 April) was 0.43. The MCRTM/CFORS model is consistent with these observations, predicting a mean AOT of 0.45 and a clear-sky surface-forcing efficiency of $-62 \pm 5 \text{ W m}^{-2}$ over the ship's track in the Sea of Japan. Together, ship and satellite observations [from the Clouds and Earth's Radiant Energy System (CERES) instrument on the *Terra* satellite] show that the ratio of the surface-to-clear-sky

TABLE 1. Calculated TOA and surface radiative forcing during 5–15 Apr 2001 over east Asia (20° – 50° N, 100° – 150° E).

	Forcing (W m^{-2})		
	Surface	Atmosphere	TOA
Dust	-9.3	3.8	-5.5
Sulfate	-3.6	0.3	-3.3
Organic carbon	-3.9	1.7	-2.2
Black carbon	-4.1	4.5	0.4
Sea salt	-0.4	0.0	-0.4
Internal mixture	-2.2	3.5	1.3
Thermal IR	3.0	-2.3	0.7
Total forcing (clear sky)	-20.5	11.5	-9.0
Total forcing (with clouds)	-14.0	11.0	-3.0

TOA forcing is 2.1 ± 0.2 , compared with the clear-sky-predicted value of 2.2.

Studies of aerosol effects on the earth's energy budget usually consider only the cooling effects at short (solar) wavelengths, but studies from the *Ronald H. Brown* demonstrate that they also have an important warming effect at thermal infrared (IR) wavelengths. Unique, high-resolution spectra obtained during the cruise were used to determine the aerosol greenhouse effect (IR radiative forcing) at the surface (Vogelmann et al. 2003) (Fig. 8). They found that the surface greenhouse effects are often a few watts per square meter and can reach almost 10 W m^{-2} for large aerosol loadings. An IR model, developed using independent aerosol and scattering measurements, confirmed this result, by producing good agreement with these observations, pyrgeometer downwelling fluxes, and IR satellite (CERES) measurements (Markowicz et al. 2003). This model was used to relate the IR aerosol forcing to the solar forcing; the surface infrared aerosol radiative forcing is between 10% and 25% of the shortwave aerosol forcing, and at the top of the atmosphere is up to 19%.

It is interesting to compare the radiative forcing measured during ACE-Asia to that seen during the Indian Ocean Experiment (INDOEX), which studied industrial and biomass emissions from south Asia as they advect over the north Indian Ocean during the Asian winter monsoon (Satheesh and Ramanathan 2000). The surface forcing observed during ACE-Asia of -14 W m^{-2} is similar to that during INDOEX, but has significantly different controlling factors. In comparison to the south Asian aerosol plumes, the east Asian plume is characterized by increased radiative scattering by dust, more pro-

nounced layering due to midlatitude frontal systems, and a greater radiative influence of high- and midlevel clouds. The mid- and upper-level clouds over east Asia reduce aerosol absorption, as opposed to the predominant low clouds that enhanced aerosol absorption during INDOEX.

CONCLUSIONS. Climatic effects of massive regional outbreaks of dust and anthropogenic aerosol are not currently known quantitatively but are likely to be both significant and complex, reflecting the opposing influences of large reductions in radiative flux reaching the earth's surface and atmospheric heating, owing to the presence of absorbing substances (such as soot). Dust provides surfaces for uptake of gas-phase species, and serves as a carrier for pollution-derived species, including sulfates, nitrates, trace metals, and carbonaceous components. Because dust reacts with sulfur dioxide and nitric acid and becomes more hygroscopic, it may play a role in regional cloud formation. This interaction of pollutant emissions and mineral dust aerosol is also expected to lead to increased solubility of Fe and other nutrients, with a

potential impact on oceanic productivity when deposited to the ocean surface. Bishop et al. (2002) report a near doubling of biomass in the ocean mixed layer over a 2-week period after the passage of this dust storm, attributed to a biotic response to the natural iron fertilization by the dust. Trace metals show evidence for the long-range transport of dust-derived minerals like Al and Fe, in addition to fossil fuel combustion indicators, such as Pb and V. Carbonaceous components play a key role in the absorbing properties of the dust, providing a proportionately stronger impact on atmospheric heating than submicrometer black carbon plays at lower altitudes, where its residence time is shorter. Application of a state-of-the-art atmospheric chemical transport model to the dust episode of 5–15 April 2001 shows the ability to capture both atmospheric vertical heterogeneity and the reduction in solar radiative fluxes at the surface. ACE-Asia can, therefore, be viewed as an important step in climate assessment, in which comprehensive remote and in situ measurements of atmospheric trace gases and aerosols were combined with models to quantify the anthropogenic alterations of atmospheric composition and properties that serve as a stimulus for climate change.

ACKNOWLEDGMENTS. This work was funded by the National Science Foundation (the lead agency for ACE-Asia), the Office of Naval Research, and NOAA. This research is a contribution to the International Global Atmospheric Chemistry (IGAC) Core Project of the International Geosphere Biosphere Program (IGBP), and is part of the IGAC Aerosol Characterization Experiments (ACE).

REFERENCES

- Arimoto, R., and Coauthors, 1996: Relationships among aerosol constituents from Asia and the North Pacific during PEM-West A. *J. Geophys. Res.*, **101**, 2011–2023.
- Bishop, J. K. B., R. E. Davis, and J. T. Sherman, 2002: Robotic observations of dust storm enhancement of carbon biomass in the North Pacific. *Science*, **298**, 817–820.
- Brechel, F. J., and G. Buzorius, 2001: Airborne observations of recent new particle formation over two urban areas in the U.S. *J. Aerosol Sci.*, **32**, S115–116.
- Carmichael, G. R., Y. Zhang, L.-L. Chen, M.-S. Hong, and H. Ueda, 1996: Seasonal variation of aerosol composition at Cheju Island, Korea. *Atmos. Environ.*, **30**, 2407–2416.
- Chun, Y., J.-Y. Kim, J. C. Choi, K. O. Boo, S. N. Oh, and M. Lee, 2001: Characterization of number size dis-

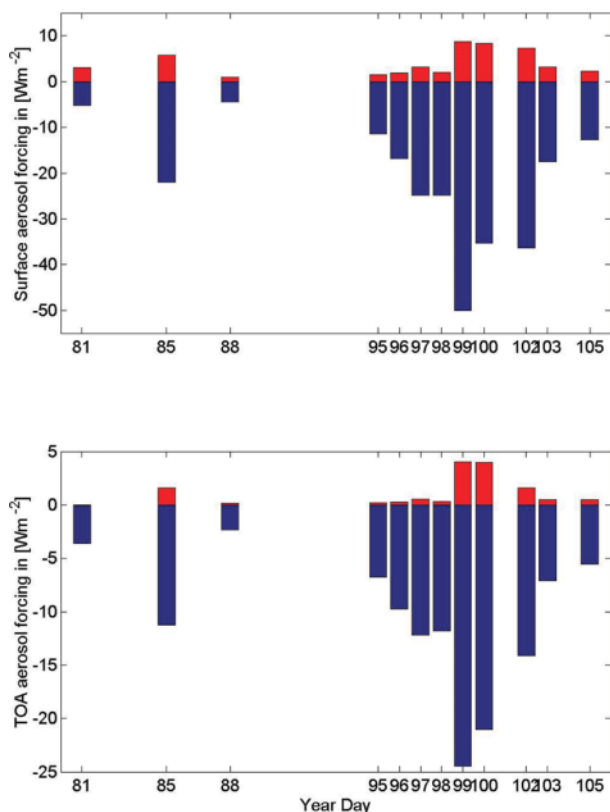


FIG. 8. Comparison between (a) the surface and (b) the TOA shortwave and IR aerosol forcing. The positive values correspond with IR forcing and negative values are for solar aerosol forcing.

- tribution of aerosol during Asian dust period in Korea. *Atmos. Environ.*, **35**, 2715–2721.
- Clarke, A. D., W. G. Collins, P. J. Rasch, V. N. Kaspustin, K. Moore, S. Howell, and H. E. Fuelberg, 2001: Dust and pollution transport on global scales: Aerosol measurements and model predictions. *J. Geophys. Res.*, **106**, 32 555–32 569.
- Eck, T. F., B. N. Holben, I. Slutsker, and A. Setzer, 1998: Measurements of irradiance attenuation and estimation of aerosol single-scattering albedo for biomass burning aerosols in Amazonia. *J. Geophys. Res.*, **103**, 31 865–31 878.
- Fernald, G., 1984: Analysis of atmospheric lidar observations: Some comments. *Appl. Opt.*, **23**, 652–653.
- Gao, Y., and J. R. Anderson, 2001: Characteristics of Chinese aerosols determined by individual-particle analysis. *J. Geophys. Res.*, **106**, 18 037–18 045.
- Grassian, V., 2001: Heterogeneous uptake and reaction of nitrogen oxides and volatile organic compounds on the surface of atmospheric particles including oxides, carbonates, soot and mineral dust: Implications for the chemical balance of the troposphere. *Int. Rev. Phys. Chem.*, **20**, 467–548.
- Hayami, H., and G. R. Carmichael, 1998: Factors influencing the seasonal variation in particulate nitrate at Cheju Island, South Korea. *Atmos. Environ.*, **32**, 1427–1434.
- Hess, M., P. Koepke, and I. Schult, 1998: Optical properties of aerosols and clouds: The software package OPAC. *Bull. Amer. Meteor. Soc.*, **79**, 831–844.
- Holden, C., Ed., 2001: The perfect dust storm. *Science*, **294**, 2469.
- Huebert, B. J., T. Bates, P. B. Russell, G. Shi, Y. J. Kim, K. Kawamura, G. Carmichael, and T. Nakajima, 2003: An overview of ACE-Asia: Strategies for quantifying the relationships between Asian aerosols and their climatic impacts. *J. Geophys. Res.*, **108**, 8633, doi:10.1029/2003JD003550.
- Jacobson, M. Z., 2000: A physically-based treatment of elemental carbon optics: Implications for global direct forcing of aerosols. *Geophys. Res. Lett.*, **27**, 217–220.
- Kaufman, Y. J., D. Tanré, O. Dubovik, A. Karnieli, and L. A. Remer, 2001: Absorption of sunlight by dust as inferred from satellite and ground-based remote sensing. *Geophys. Res. Lett.*, **28**, 1479–1482.
- Kim, Y. P., J. H. Lee, N. J. Baik, J. Y. Kim, S.-G. Shim, and C.-H. Kang, 1998a: Summertime characteristics of aerosol composition at Ceju Island, Korea. *Atmos. Environ.*, **32**, 3905–3915.
- , S.-G. Shim, K. C. Moon, C.-G. Hu, C.-H. Kang, and K. Y. Park, 1998b: Monitoring of air pollutants at Kosan, Ceju Island, Korea, during March–April 1994. *J. Appl. Meteor.*, **37**, 1117–1126.
- Maria, S. F., L. M. Russell, B. J. Turpin, and R. J. Porcja, 2002: FTIR measurements of functional groups and organic mass in aerosol samples over the Caribbean. *Atmos. Environ.*, **36**, 5185–5196.
- Markowicz, K. M., P. J. Flatau, A. M. Vogelmann, P. K. Quinn, and E. J. Welton, 2003: Clear-sky infrared aerosol radiative forcing at the surface and the top of the atmosphere. *Quart. J. Roy. Meteor. Soc.*, **129**, 2927–2947.
- Michel, A. E., C. R. Usher, and V. H. Grassian, 2002: Heterogeneous and catalytic uptake of ozone on mineral oxides and dusts: A Knudsen cell investigation. *Geophys. Res. Lett.*, **29**, 1665, doi:10.1029/2002GL014896.
- Nishikawa, M., Q. Hao, and M. Morita, 2000: Preparation and evaluation of certified reference materials for Asian mineral dust. *Global Environ. Res.*, **4**, 103–113.
- Nriagu, J. O., and J. M. Pacyna, 1988: Quantitative assessment of worldwide contamination of air, water and soils by trace metals. *Nature*, **333**, 134–139.
- Orsini, D. A., Y. Ma, A. Sullivan, B. Sierau, K. Baumann, and R. J. Weber, 2003: Refinements to the Particle-Into-Liquid Sampler (PILS) for ground and airborne measurements of water soluble aerosol composition. *Atmos. Environ.*, **37**, 1243–1259.
- Pielke, R. A., and Coauthors, 1992: A comprehensive meteorological modeling system—RAMS. *Meteor. Atmos. Phys.*, **49**, 69–91.
- Podgorny, I., W. C. Conant, V. Ramanathan, and S. K. Satheesh, 2000: Aerosol modulation of atmospheric and surface solar heating over the tropical Indian Ocean. *Tellus*, **52B**, 947–958.
- Raes, F., T. Bates, F. McGovern, and M. Van Liedekerke, 2000: The 2nd aerosol characterization experiment (ACE-2): Meteorological and chemical context. *Tellus*, **52B**, 111–125.
- Ramanathan, V., P. J. Crutzen, J. T. Kiehl, and D. Rosenfeld, 2001: Aerosols, climate, and the hydrological cycle. *Science*, **294**, 2119–2124.
- Russell, P. B., and Coauthors, 1999: Aerosol-induced radiative flux changes off the United States mid-Atlantic coast: Comparison of values calculated from Sun photometer and in situ data with those measured by airborne pyranometer. *J. Geophys. Res.*, **104**, 2289–2307.
- Satheesh, S. K., and V. Ramanathan, 2000: Large differences in tropical aerosol forcing at the top of the atmosphere and Earth's surface. *Nature*, **405**, 60–63.
- Streets, D. G., K. Jiang, X. Hu, J. E. Sinton, X.-Q. Zhang, D. Xu, M. Z. Jacobson, and J. E. Hansen, 2001: Recent reductions in China's greenhouse gas emissions. *Science*, **294**, 1835–1837.

- Sugimoto, N., I. Uno, M. Nishikawa, A. Shimizu, I. Matsui, X. Dong, Y. Chen, and H. Quan, 2003: Record heavy Asian dust in Beijing in 2002: Observations and model analysis of recent events. *Geophys. Res. Lett.*, **30**, 1640, doi:10.1029/2002GL016349.
- Uno, I., 2003: Regional chemical weather forecasting system CFORS: Model descriptions and analysis of surface observations at Japanese island stations during the ACE-Asia experiment. *J. Geophys. Res.*, **108**, 8668, doi:10.1029/2002JD002845.
- Van Curen, R. A., and T. A. Cahill, 2002: Asian aerosols in North America: Frequency and concentration of fine dust. *J. Geophys. Res.*, **107**, 4804, doi:10.1029/2002JD002204.
- Vogelmann, A. M., V. Ramanathan, and I. Podgorny, 2001: Scale dependence of solar heating rates in convective cloud systems with implications to general circulation models. *J. Climate*, **14**, 1738–1752.
- , P. J. Flatau, M. Szczodrak, K. M. Markowicz, and P. J. Minnett, 2003: Observations of large aerosol infrared forcing at the surface. *Geophys. Res. Lett.*, **30**, 1655, doi:10.1029/2002GL016829.
- Weber, R. J., D. Orsini, Y. Daun, Y.-N. Lee, P. J. Klotz, and F. Brechtel, 2001: A particle-into-liquid collector for rapid measurement of aerosol bulk chemical composition. *Aerosol Sci. Technol.*, **35**, 718–727.
- , and Coauthors, 2003: New particle formation in anthropogenic plumes advecting from Asia observed during TRACE-P. *J. Geophys. Res.*, **106**, 8814, doi:10.1029/2002JD003112.